Int. J. Heat Mass Transfer. Vol. 34, No. 6, pp. 1371–1382, 1991
Printed in Great Britain

0017–9310/91 $3.00 + 0.00

Natural convection in a horizontal annulus partially filled with cold water

C. J. HO
Department of Mechanical Engineering, National Cheng Kung University, Tainan, Taiwan 70101, R.O.C.

and

Y. H. LIN
Department of Mechanical Engineering, National Pintung Institute of Agriculture, Pintung, Taiwan 91207, R.O.C.

(*Received* 25 *April* 1990 *and in final form* 25 *June* 1990)

Abstract—A combined numerical and experimental study is reported of natural convection inside a horizontal concentric cylindrical annulus partially filled with cold water encompassing the density inversion. A holographic interferometry system is employed to map the temperature distribution in the water layer, and a laser shadowgraph system is used to measure the local heat transfer coefficient on the water-wetted inner cylinder of the annulus. Numerical simulations have also been conducted for the steady, laminar natural convection of air/water layers enclosed in the annulus. Both the numerical and the experimental results obtained in the present study unveil an interesting coupling between the natural convection of the air layer and that of the cold water bulk in the presence of the density inversion effect. The predictions are in good agreement with the experimental data.

INTRODUCTION

IT IS WELL known that pure water exhibits a density extreme at 4°C under atmospheric pressure. Buoyancy-driven flows of water encompassing the density extreme (cold water) are of fundamental interest due to their relevance to numerous engineering and geophysical applications. A recent review of research advances in natural convection of cold water by Gebhart [1] clearly points out that relatively few efforts have been devoted to this area. Of interest in the present study is natural convection heat transfer in a horizontal concentric cylindrical annulus partially filled with cold water, as depicted schematically in Fig. 1. Having an air layer atop the water layer as shown in Fig. 1, a two-fluid natural convection situation arises in the annulus. The presence of the air/water interface can complicate the flow structures as well as the heat transfer characteristics of natural convection in the two-fluid annulus. So far relatively few works have been reported that deal with two-fluid natural convection in enclosures. Detailed surveys of these early studies can be found in refs. [2–4]. Of direct relevance to the physical configuration considered in the present work are those of refs. [3, 4]. Projahn and Beer [3] conducted a numerical investigation on laminar combined buoyancy- and thermocapillary-driven convection in horizontal cylindrical annuli filled with four pairs of immiscible fluids. The authors recently extended the study of ref. [3] to investigate the influence of mixed thermal boundary conditions as well as interfacial heat exchange characteristics in horizontal cylindrical annuli filled with air/water layers [4]. However, the numerical works reported in refs. [3, 4] are rather restricted to the situations of which the fluid–fluid interface always coincides with the horizontal centreline of the inner cylinder of the annulus.

The work reported in this paper represents a continuing effort to expand the existing knowledge concerning the two-fluid natural convection; the main

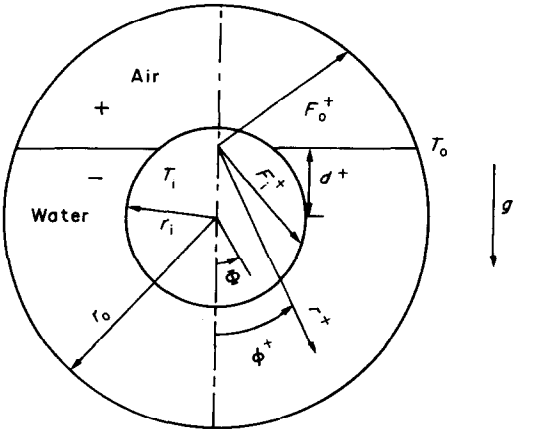

FIG. 1. Schematic diagram of the physical configuration and coordinate system.

NOMENCLATURE

a	exponent in the density equation
A	heat transfer area
d^+	distance of the air/water interface away from the horizontal centreline of the annulus
d	dimensionless distance, d^+/L
F_i^+	radial profile of inner cylinder
F_i	dimensionless radial profile of inner cylinder, F_i^+/L
F_o^+	radial profile of outer cylinder
F_o	dimensionless radial profile of outer cylinder, F_o^+/L
g	gravitational acceleration
h	heat transfer coefficient
k	thermal conductivity
L	gap of the annulus, $(r_o - r_i)$
Nu	Nusselt number
Pr_-	Prandtl number, (ν_-/α_-)
r^+	radial coordinate
r	dimensionless radial coordinate, r^+/L
Ra_-	Rayleigh number, $g\, rsp\, L^3(T_i - T_o)^a/(\nu_-\alpha_-)$
r_i	radius of inner cylinder
R_i	dimensionless radius of inner cylinder, r_i/L
r_o	radius of outer cylinder
R_o	dimensionless radius of outer cylinder, r_o/L
rsp	coefficient in density equation
T	temperature
u	radial velocity component
v	angular velocity component.

Greek symbols

α	thermal diffusivity
β	thermal expansion coefficient
γ	density inversion parameter, $(T_m - T_o)/(T_i - T_o)$
η	radial coordinate in transformed plane
θ	dimensionless temperature, $(T - T_o)/(T_i - T_o)$
μ	absolute viscosity
ν	kinematic viscosity
ρ	density
Φ	angular coordinate centred at the inner cylinder
ϕ^+	angular coordinate
ϕ	dimensionless angular coordinate, ϕ^+/π
ψ^+	stream function
ψ	dimensionless stream function, ψ^+/α_-
ω^+	vorticity
ω	dimensionless vorticity, $\omega^+ L^2/\alpha_-$.

Subscripts

+, −	upper (air) and lower (water) layer, respectively
i, o	inner and outer cylinder, respectively
s	ratio of the quantity for the lower to the upper fluid.

Superscript

¯	circumferentially averaged quantity.

objective is to shed light on the effect of density inversion in the cold water layer on the air/water natural convective fluid flow and heat transfer in enclosures. A series of numerical simulations via a finite difference method has been performed for the physical configuration under consideration. The numerical simulations are supplemented by experiments in a horizontal concentric cylindrical annulus filled with various volumetric fractions of the water layer. Temperature distributions in the water bulk were mapped by means of a holographic interferometry system. A laser shadowgraph system was used to measure the local heat transfer coefficient along the water-wetted portion of the inner cylinder of the annulus. The numerical results are validated through comparisons with the corresponding experimental data.

ANALYSIS

Model equations

As shown in Fig. 1, the coordinate system selected for the mathematical formulation of the physical problem considered here has its origin located at the midpoint of the air/water interface. The air/water interface is assumed flat and the influence of the curved meniscus at the fluid–solid interface is neglected. The location of the interface is designated by its positive/negative distance, d^+, below/above the horizontal centreline of the concentric annulus. The outer and inner cylinders of the annulus are maintained as the cold and hot isothermal surfaces, respectively.

The fluid flow developed in the air/water layer enclosed in the annulus is assumed to be two-dimensional, steady, laminar, incompressible, and the Boussinesq approximation is invoked. The properties, except for the density in buoyancy force terms, are assumed temperature independent. Effects of vaporization/condensation and mass transfer at the interface are neglected. The viscous dissipation and compressibility effects are also assumed negligible. Moreover, symmetry with respect to the vertical midplane through the axis of the cylinders is assumed in order to reduce the computational effort.

To circumvent the difficulty of an irregular solution domain encountered in the situation in which the annulus is not half-filled with water, namely the air/water interface is not flush with the horizontal

centreline of the annulus, a radial coordinate stretching transformation is incorporated in the present paper to map the domains occupied by either fluid into a half circle, respectively, in the (η, ϕ) plane where

$$\eta = \frac{r - F_i(\pi\phi)}{F_o(\pi\phi) - F_i(\pi\phi)}. \quad (1)$$

In equation (1) $F_i(\pi\phi)$ and $F_o(\pi\phi)$, respectively, are the radial profiles of the inner and outer cylinders measured from the mid-point of the air/water interface and are given as

$$F_i(\pi\phi) = [R_i^2 - d^2 \sin^2(\pi\phi)]^{1/2} - d\cos(\pi\phi) \quad (2a)$$

and

$$F_o(\pi\phi) = [R_o^2 - d^2 \sin^2(\pi\phi)]^{1/2} + d\cos(\pi\phi). \quad (2b)$$

Using the foregoing transformation, equation (1), the restriction of the air/water interface being always flush with the horizontal centreline of the annulus imposed in the previous numerical analyses [3, 4] can be readily relaxed to a greater extent that the interface position may be varied as long as the interface remains in contact with the inner cylinder of the annulus.

With the foregoing assumptions, in the transformed domain the dimensionless governing equations for the physical configuration considered can be written in terms of vorticity, stream function, and temperature as:

vorticity equation

$$\frac{1}{\pi r}\frac{\partial\eta}{\partial r}\left(\frac{\partial\psi}{\partial\phi}\frac{\partial\omega}{\partial\eta} - \frac{\partial\psi}{\partial\eta}\frac{\partial\omega}{\partial\phi}\right) = Pr\_(B\nabla^2\omega + C\,Ra\_\,S) \quad (3)$$

stream function equation

$$\nabla^2\psi = -\omega \quad (4)$$

energy equation

$$\frac{1}{\pi r}\frac{\partial\eta}{\partial r}\left(\frac{\partial\psi}{\partial\phi}\frac{\partial\theta}{\partial\eta} - \frac{\partial\psi}{\partial\eta}\frac{\partial\theta}{\partial\phi}\right) = D\nabla^2\theta \quad (5)$$

where

$$\nabla^2 \equiv \left[\left(\frac{\partial\eta}{\partial r}\right)^2 + \left(\frac{1}{\pi r}\frac{\partial\eta}{\partial\phi}\right)^2\right]\left(\frac{\partial^2}{\partial\eta^2}\right) + \frac{2}{(\pi r)^2}\frac{\partial\eta}{\partial\phi}\frac{\partial^2}{\partial\eta\partial\phi} + \frac{1}{(\eta r)^2}\frac{\partial^2}{\partial\phi^2} + \left[\frac{1}{r}\frac{\partial\eta}{\partial r} + \frac{1}{(\eta r)^2}\frac{\partial^2\eta}{\partial\phi^2}\right]\frac{\partial}{\partial\eta} \quad (6a)$$

$$\frac{\partial\eta}{\partial r} = \frac{1}{F_o - F_i} \quad (6b)$$

$$\frac{\partial\eta}{\partial\phi} = \frac{-1}{F_o - F_i}\left[\eta\frac{\partial F_o}{\partial\phi} + (1-\eta)\frac{\partial F_i}{\partial\phi}\right] \quad (6c)$$

$$\frac{\partial^2\eta}{\partial\phi^2} = \frac{-1}{F_o - F_i}\left[\eta\frac{\partial^2 F_o}{\partial\phi^2} + 2\frac{\partial\eta}{\partial\phi}\frac{\partial F_o}{\partial\phi} - 2\frac{\partial\eta}{\partial\phi}\frac{\partial F_i}{\partial\phi} + (1-\eta)\frac{\partial^2 F_i}{\partial\phi^2}\right] \quad (6d)$$

and for the water layer, $(0 \leqslant \phi \leqslant \frac{1}{2})$

$$B = 1, \quad C = 1, \quad D = 1,$$

$$S = \sin(\pi\phi)\frac{\partial\eta}{\partial\phi}\frac{\partial}{\partial\eta}|\theta - \gamma|^a + \frac{\cos(\pi\phi)}{\pi r}\left(\frac{\partial}{\partial\phi}|\theta-\gamma|^a + \frac{\partial\eta}{\partial\phi}\frac{\partial}{\partial\eta}|\theta-\gamma|^a\right) \quad (6e)$$

and for the air layer, $(\frac{1}{2} \leqslant \phi \leqslant 1)$

$$B = \frac{1}{\nu_s}, \quad C = \beta^*, \quad D = \alpha_s,$$

$$S = \sin(\pi\phi)\frac{\partial\eta}{\partial r}\frac{\partial\theta}{\partial\eta} + \frac{\cos(\pi\phi)}{\pi r}\left(\frac{\partial\theta}{\partial\phi} + \frac{\partial\eta}{\partial\phi}\frac{\partial\theta}{\partial\eta}\right). \quad (6f)$$

The buoyancy terms in the vorticity equation, equation (6e), for the water layer are based on a non-linear density–temperature relation for cold water proposed by Gebhart and Mollendorf [5]

$$\rho(T) = \rho_m(1 - rsp|T - T_m|^a) \quad (7)$$

where $\rho_m = 999.9720$ kg m^{-3}, $rsp = 9.297173 \times 10^{-6}(°C)^{-a}$, $T_m = 4.029325°C$, and $a = 1.894816$.

The dimensionless boundary conditions for the problem may be stated as

$$\psi = \omega = \frac{\partial\theta}{\partial\phi} = 0$$

$$\text{at} \quad \phi = 0 \text{ or } 1 \text{ (symmetry line)} \quad (8a)$$

$$\psi = \frac{\partial\psi}{\partial\eta} = 0, \quad \theta = 0 \quad \text{at} \quad \eta = 1, \quad 0 \leqslant \phi \leqslant 1 \quad (8b)$$

$$\psi = \frac{\partial\psi}{\partial\eta} = 0, \quad \theta = 1 \quad \text{at} \quad \eta = 0, \quad 0 \leqslant \phi \leqslant 1. \quad (8c)$$

In addition, the conditions at the air/water interface are given by

$$\theta_+ = \theta_- \quad (9a)$$

$$u_+ = u_- \quad (9b)$$

$$v_+ = v_- = 0 \quad (9c)$$

$$\left(\frac{\partial\theta}{\partial\phi} + \frac{\partial\eta}{\partial\phi}\frac{\partial\theta}{\partial\eta}\right)_+ = k_s\left(\frac{\partial\theta}{\partial\phi} + \frac{\partial\eta}{\partial\phi}\frac{\partial\theta}{\partial\eta}\right)_- \quad (9d)$$

$$\frac{1}{\mu_s}\left(\frac{\partial u}{\partial\phi} + \frac{\partial\eta}{\partial\phi}\frac{\partial u}{\partial\eta}\right)_+ = \left(\frac{\partial u}{\partial\phi} + \frac{\partial\eta}{\partial\phi}\frac{\partial u}{\partial\eta}\right)_-. \quad (9e)$$

It should be noted that in the continuity condition of the interfacial shear, equation (9e), the surface tension effect is neglected in considering the size of the test cell used in the experimental part of the current study [2].

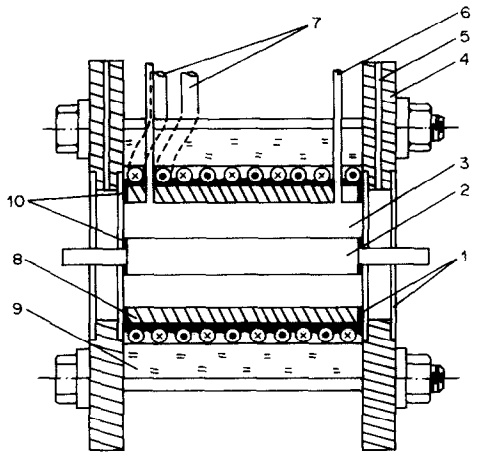

FIG. 2. Schematic diagram of the test cell: 1, window of glass; 2, cylindrical heat exchanger; 3, annular cavity (test region); 4, fixer; 5, vacuum tube; 6, compensating tube; 7, cooling coil; 8, copper cylinder; 9, insulator of packed fibre; 10, O-ring.

The foregoing formulation for the problem considered here clearly reveals that the fluid flow and heat transfer of the air/water layer enclosed in the annulus are governed by the following dimensionless parameters: the Rayleigh number, Ra, the Prandtl number, Pr_-, the density parameter, γ, the parameter, $\beta^*(=\beta_+(T_i-T_o)^{1-a}/rsp)$, the radius ratio, r_o/r_i, and the dimensionless distance, d, designating the position of the air/water interface.

Solution method

The field equations (3)–(5), together with the boundary conditions and interfacial conditions, equations (8) and (9), were solved numerically utilizing a finite difference method. The field equations were discretized on a non-uniform mesh system having a denser grid near both the solid boundaries of the annulus and the air/water interface. The derivatives in the field equations were approximated by the second-order central difference scheme except for the convective terms for which a two-dimensional QUICK scheme [6] was employed.

The steady-state solutions to the finite difference equations were then obtained through an iterative procedure. The details of the calculation procedure are essentially the same as those described in the earlier study [4] and do not need to be repeated here. After performing sensitivity tests with different grids, a non-uniform mesh system of 35(radial) by 31 (angular) grid points was respectively chosen for the air and water layer as a compromise between cost and accuracy.

EXPERIMENTS

Experiments were performed in a well-insulated test cell of horizontal concentric cylindrical annular cross section, partially filled with distilled water as shown schematically in Fig. 2. The annular test cell consists mainly of an outer brass tube of inner diameter 15.2 cm, 9.6 cm in depth, and an inner cylinder of outer diameter 5.8 cm, yielding a nominal radius ratio of 2.60. The outer tube is wrapped by a heat exchanger coil which is soldered to the outer surface of the tube. Outside the heat exchanger coil a 5 cm thick blanket of foam insulation material is utilized to minimize heat exchange with the ambient environment. The inner cylinder is a multipass heat exchanger machined out of a brass rod. The constant isothermal surface temperatures at the inner and outer cylinders of the annulus were fulfilled through circulating thermally regulated fluid (a mixture of ethanol in water) from two constant temperature baths, respectively. The outer/inner surface temperatures of the inner/outer cylinder were measured with four copper–constantan thermocouples epoxied separately into small-diameter holes located 90 deg apart angularly, which were drilled close to the inner surface of the annular test cell facing the air/water layer. In addition, another six thermocouples were positioned longitudinally along the surfaces of the inner and outer cylinders to monitor the temperature uniformity in the longitudinal direction of the test cell. In all experiments, the surface temperatures in the annular test section were uniform to within $\pm 0.1^\circ$C angularly and $\pm 0.2^\circ$C longitudinally of the desired temperature.

Double-pane glass windows were used as front and back walls for the test cell to permit access for optical measurements. Moreover, the gaps inside the double-pane windows were evacuated by a vacuum pump prior to each experiment to further reduce heat exchange with the ambient.

A technique of real-time holographic interferometry [7] with 15 cm optics was utilized for mapping the qualitative temperature field in the annular test cell. The adjustment of initial infinite fringe field was employed for the experiments and therefore the interference fringes obtained are equivalent to the isotherms in the fluid [8]. Moreover, a laser shadowgraph system was constructed to measure the local heat coefficient along the heated inner cylinder. Due to the distinct difference in the refractive indices of air and water, the optical measurements with the designed test cell could only be carried out for the water layer. The evaluation procedure for the shadowgraph measurements involved with cold water is the same as that described in ref. [9] which measured the heat transfer coefficient during melting of ice around a horizontal heated cylinder.

The experiments were conducted in a regular sequence, starting with the uppermost position of the air/water interface, namely the case when the annulus is full of water, $d = -1.625$, and proceeding then toward lower and lower interface positions. Moreover, the experiments for natural convection in the annulus filled with air were carried out and agree well with the interferometric results of Kuehn and Goldstein [10], lending validation for the interferometric measurements of the present study.

RESULTS AND DISCUSSION

Numerical predictions

The numerical results have been obtained for an annulus of radius ratio fixed at 2.6, Ra_- up to 10^6, γ between 0 and 1, and d from -0.620 to 0.620. It should be underlined that all solutions presented here were found with β^* fixed at 0.036 since the solutions in the aforementioned ranges of Ra_-, γ, and d appear to be insensitive to variation of β^* in the range of 0.036–0.1 corresponding to the temperature difference ranges considered in the present study.

First of all, the flow structures and temperature distributions developed in both air and water layers enclosed in the annulus will be respectively presented by means of contour maps of streamlines on the right half of the annulus and isotherms on the left half. Figure 3 shows representative results for the annuli half-filled with water ($d = 0$) at three different values of the density inversion parameter with $Ra_- = 10^4$ and 10^6. As is expected, the clockwise recirculating flow developed in the air layer is stronger than that in the water region as indicated by the considerably smaller magnitude of the stream function in the water layer. Furthermore, it can be seen from Fig. 3 that for fixed Ra_- with an increase of the density inversion parameter, the flow structure in the air layer remains rather unchanged while a typical evolution of the flow pattern toward a completely reversed buoyant circulation (convective inversion) is clearly observed in the water bulk. On the other hand, with a fixed inversion parameter, the increase of the Rayleigh number appears to promote the density inversion effect. For instance, with $\gamma = 0.4$, shown in Fig. 3, the bicellular flow structure of approximately equal strength and size in the water bulk at $Ra_- = 10^4$ is seen to evolve into the one dominated by the counter-clockwise circulation near the outer cylinder (outer circulation) at $Ra_- = 10^6$, indicative evidently of the enhanced density inversion phenomenon. This may be rationalized by the fact that with increasing Rayleigh number, the intensified convective flow leads to develop a distinctive thermal boundary layer along the air-wetted inner cylinder and hence, due to the requirement of no thermal jump across the air/water interface, causes the density extreme isotherm in the water region to shift toward the inner cylinder at a given inversion parameter. Moreover, another important fact one can infer from the isotherms in Fig. 3 is that with a fixed Rayleigh number, the temperature field in the air region may be significantly affected by the occurrence of the density inversion phenomenon in the water bulk with increasing inversion parameter. At $Ra_- = 10^4$ as the inversion parameter is increased up to 0.8 the thermal boundary layer along the air-wetted inner cylinder becomes thinner as evidenced by the clustering of isotherms there, hence yielding enhanced heat transfer. In all, the foregoing reflects clearly an interesting coupling of the natural convection phenomenon between the air and water layers enclosed in the annulus. Of further interest revealed in Fig. 3 is the appearance of two intense thermal plumes emanating respectively from the top and bottom of the inner cylinder in the air and water layer at $Ra_- = 10^6$ with $\gamma \geqslant 0.4$.

Figures 4 and 5 are intended to illustrate the influence of the changing air/water interface location on the flow structures and isotherm patterns with $Ra_- = 19490$ for two values of the density inversion parameter. An overview of these figures reveals that regardless of the variation of the density inversion parameter the recirculating flow in the air region as expected intensifies with lowering of the air/water interface from the top of the inner cylinder as indicated by the increasing magnitude of the dimensionless stream function. As for the water layer, the influence of the interface position is rather a function of the density inversion parameter. For $\gamma = 0.2$, Fig. 4, as an ordinary fluid the flow structure in the water region remains dominated by a clockwise circulation although markedly weaker when the air/water interface position is lowered. Moreover, the isotherm patterns indicate that the diminishing water layer becomes stably stratified. With a higher value of the inversion parameter, $\gamma = 0.5$ shown in Fig. 5, the lowering of the interface induces stronger convection in the air layer, thus thinning the thermal boundary layer on the air-wetted portion of the inner cylinder. It follows that the density extreme isotherm in the water bulk shifts accordingly inward and as a result the density inversion effect becomes more pronounced as witnessed by the changing from a bicellular flow structure for $d = -0.62$ (Fig. 5) into nearly convective inversion at $d = 0.3125$.

Next, the results for the local heat transfer rate along the surfaces of the annulus are examined in terms of Nusselt numbers on the inner and outer cylinder defined respectively as

$$Nu_i = -E\left[1+\left(\frac{1}{\pi F_i}\frac{\partial F_i}{\partial \phi}\right)^2\right]^{1/2}\frac{\partial \eta}{\partial r}\frac{\partial \theta}{\partial \eta}\bigg|_{\eta=0} \tag{10a}$$

$$Nu_o = E\left[1+\left(\frac{1}{\pi F_o}\frac{\partial F_o}{\partial \phi}\right)^2\right]^{1/2}\frac{\partial \eta}{\partial r}\frac{\partial \theta}{\partial \eta}\bigg|_{\eta=1} \tag{10b}$$

where

$$E = \begin{cases} k_s & \text{for the air-wetted portion} \\ 1 & \text{for the water-wetted portion.} \end{cases}$$

In Fig. 6 the typical variations of the local Nusselt number along the inner cylinder are elucidated for a half-filled annulus ($d = 0$) with various density inversion parameters at $Ra_- = 10^4$ and 10^6. For $Ra_- = 10^4$ and $\gamma = 0.2$, it is evident from the figure that the local Nusselt number decreases gradually from the bottom reaching a flat minimum near the interface. Because of the lower thermal conductivity of the air layer above the interface, a sudden drop-off of the local Nusselt number across the interface occurs as indicated by a much smaller scale used for the right

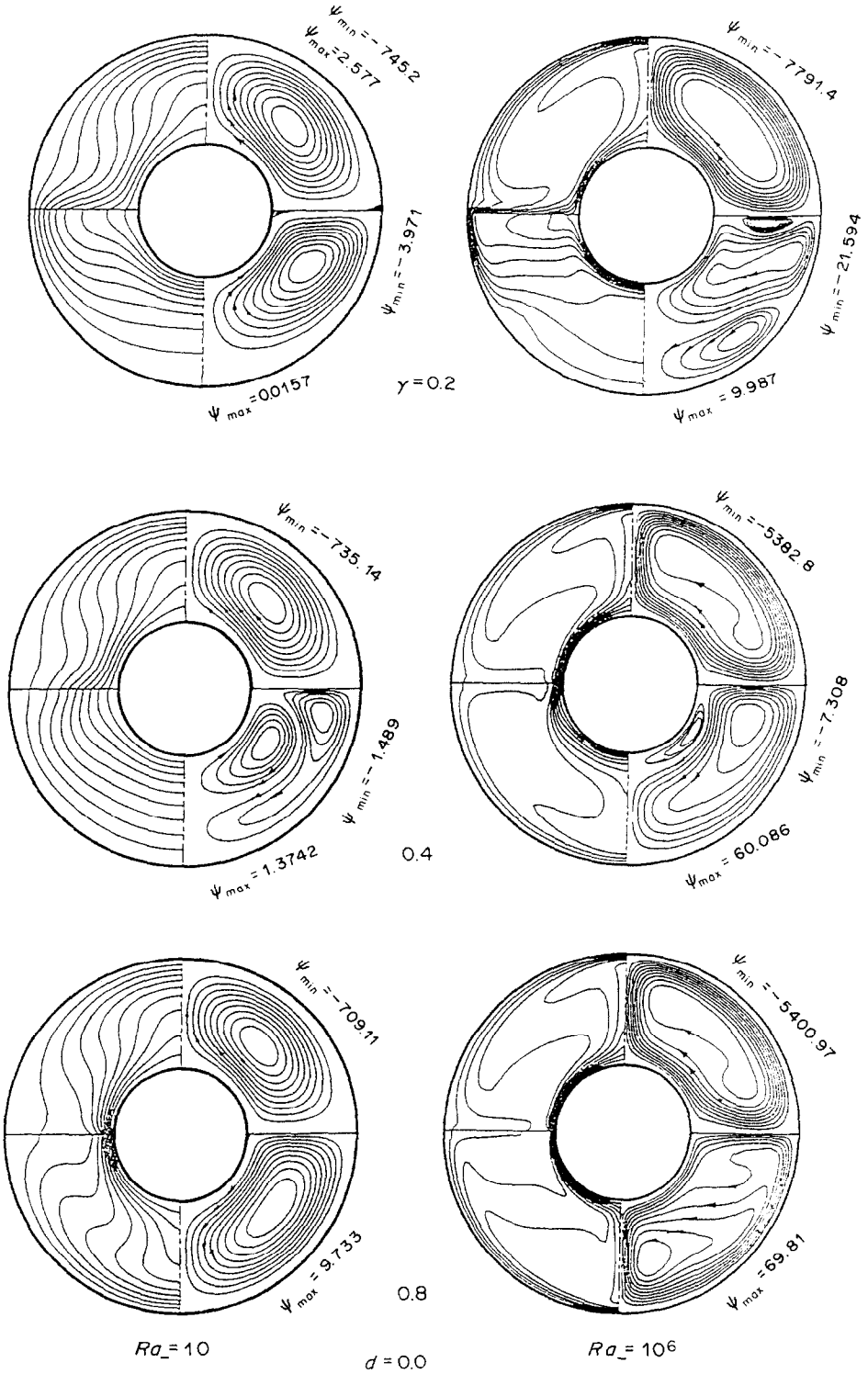

FIG. 3. Predicted flow structures and isotherms for a half-filled annulus at various density inversion parameters.

half of Fig. 6. Beyond the interface the local Nusselt number of the inner cylinder exhibits an increasing trend reaching a local maximum before a decreasing trend is resumed toward the top of the inner cylinder. As γ is increased to 0.8, the trend of the water-wetted local Nusselt number appears to be reversed, indicative of the occurrence of the convective inversion phenomenon. Meanwhile, across the interface the air-

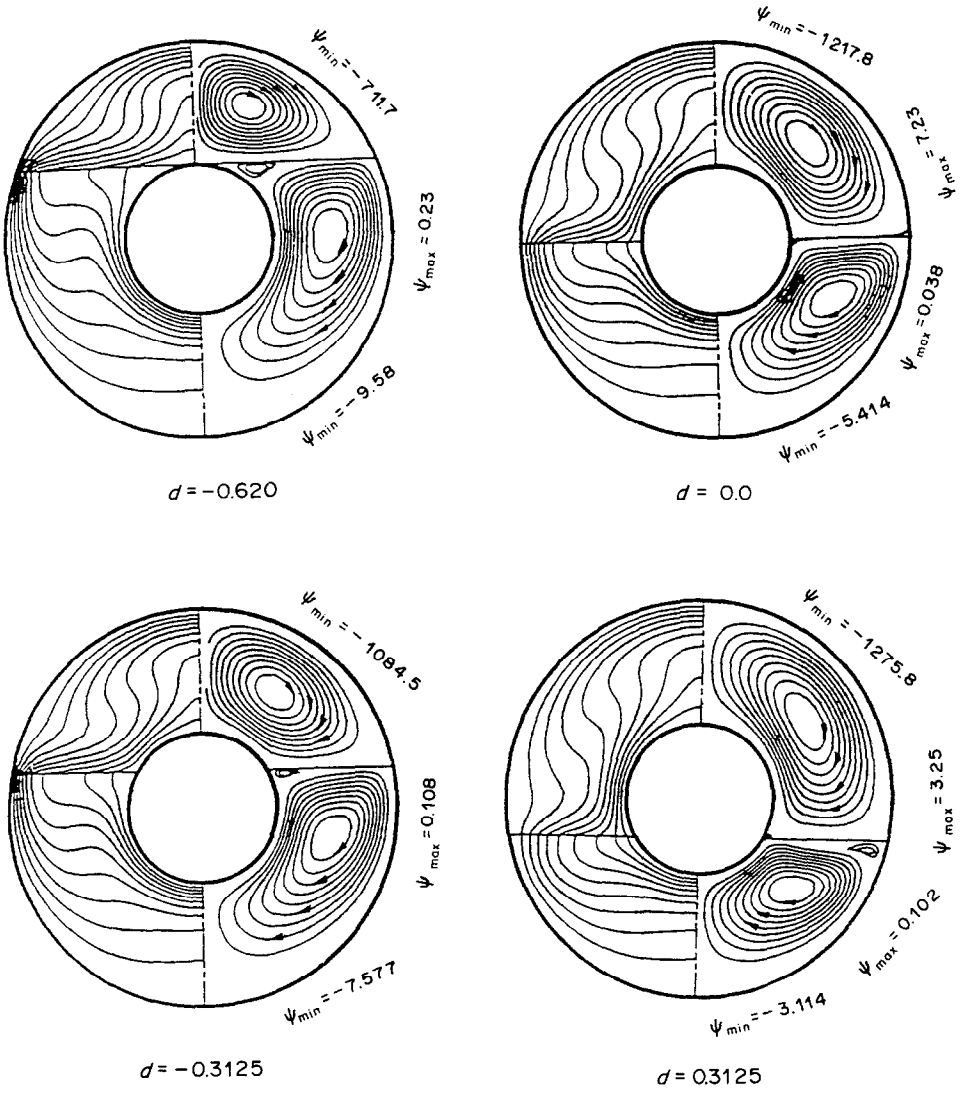

FIG. 4. Influence of air/water interface position on flow fields and isotherms at $Ra_- = 19490$ and $\gamma = 0.2$.

wetted local Nusselt number displays a monotonic decreasing trend. Moreover, it can be seen from Fig. 6 that an increase of the density inversion parameter can lead to a markedly enhanced local heat transfer rate on the air-wetted part of the inner cylinder. This is consistent with the observation elaborated in Fig. 3 of thinning of the thermal boundary layer in the air-wetted portion due to the changing flow structure in the water bulk related to density inversion. In addition, with increasing Rayleigh number the aforementioned features of the local Nusselt number on the inner cylinder become more distinctive.

Figure 7 shows the variation of local Nusselt number on the outer cylinder under the same conditions as those for Fig. 6. An inspection of the figure reveals that the local heat flux distribution along the outer cylinder qualitatively exhibits a trend opposite to that depicted in Fig. 6 for the inner cylinder.

Attention will now be turned to the average heat transfer results on the inner cylinder, for which the predicted results will be presented in dimensionless forms as average Nusselt numbers defined respectively as

$$\overline{Nu}_- = \frac{\bar{h}_- L}{k_-} = \frac{1}{(A_i)_-}\int_{(A_i)_-} Nu_i \, dA_i \qquad (11a)$$

$$\overline{Nu}_+ = \frac{\bar{h}_+ L}{k_+} = \frac{1}{(A_i)_+}\int_{(A_i)_+} Nu_i \, dA_i. \qquad (11b)$$

Figure 8 conveys the typical presentation of the average Nusselt numbers defined above against the density inversion parameter for the case half-filled with water. As seen in Fig. 8(a), on the water-wetted part of the inner cylinder a minimum average heat transfer rate arises at $\gamma = 0.4$ which is smaller than the cor-

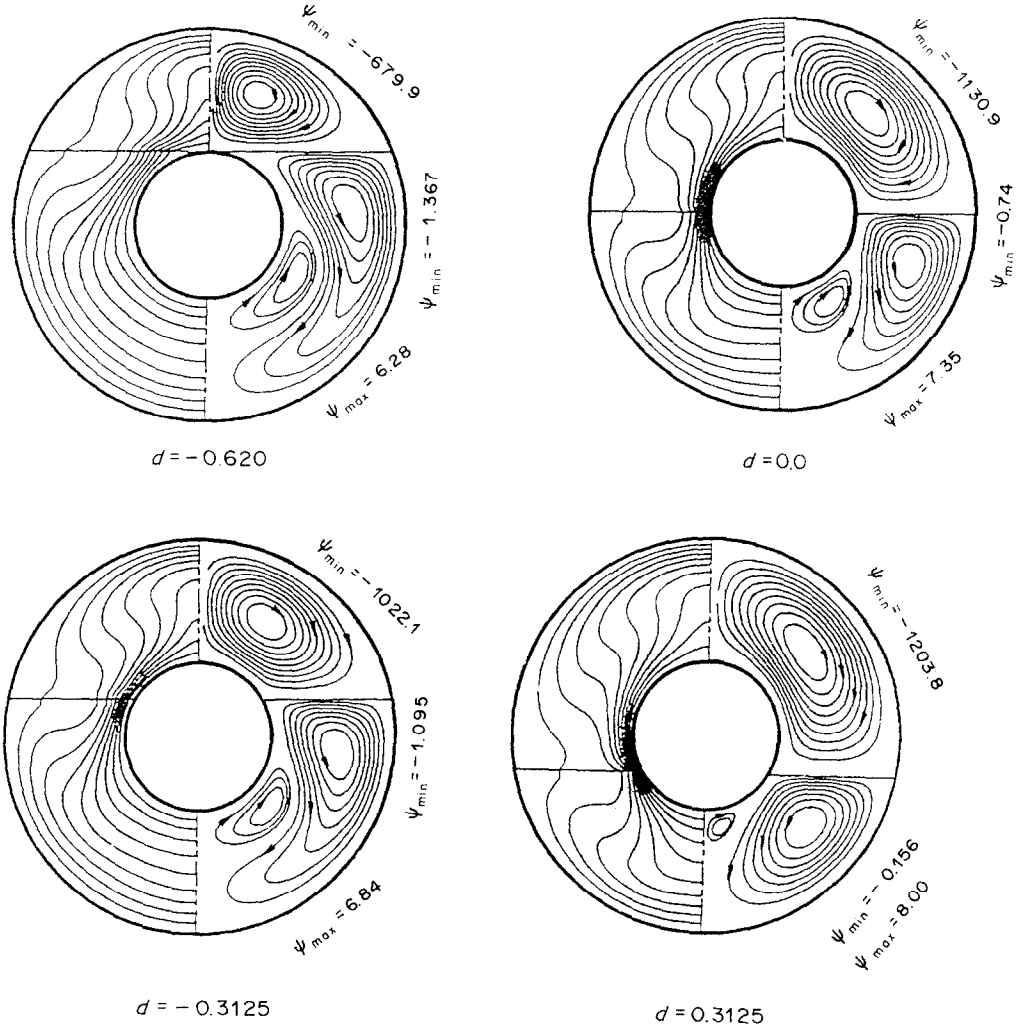

FIG. 5. Influence of air/water interface position on flow fields and isotherms at $Ra = 19\,490$ and $\gamma = 0.5$.

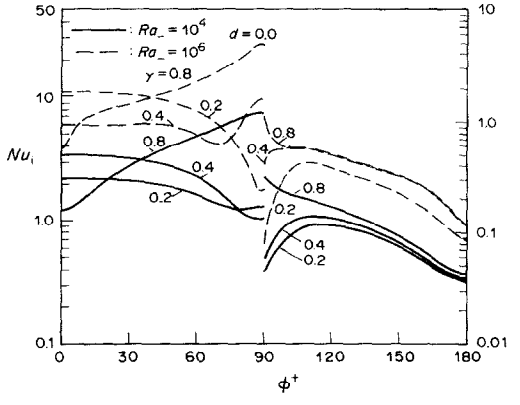

FIG. 6. Distribution of local Nusselt number on the inner cylinder of a half-filled annulus.

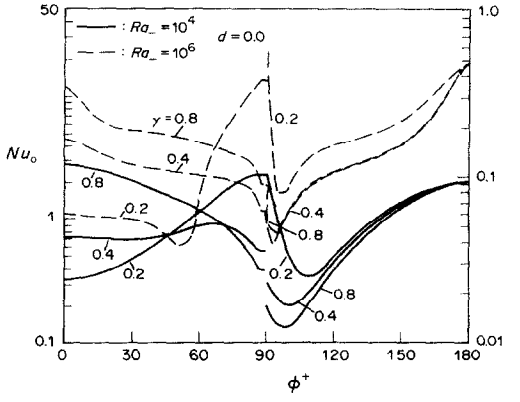

FIG. 7. Distribution of local Nusselt number on the outer cylinder of a half-filled annulus.

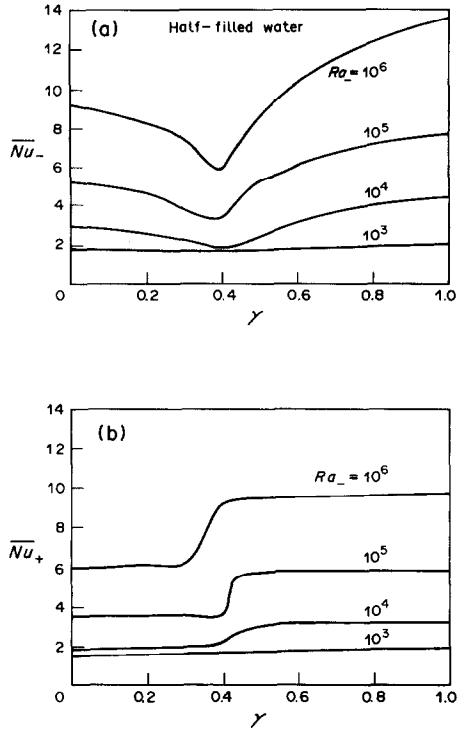

FIG. 8. Relations of average Nusselt number on the inner cylinder with the density inversion parameter: (a) water-wetted portion; (b) air-wetted portion.

responding critical value of approximately 0.44 predicted for the case filled full with water [11]. Further, such a critical value of the inversion parameter appears to be insensitive to the variation of the Rayleigh number for $Ra_- \geqslant 10^4$. As for the air-wetted portion, it is interesting to notice from Fig. 8(b) that for $Ra_- \geqslant 10^4$ the air-wetted average Nusselt number experiences a step-function-like increase as the inversion parameter is increased past a value of around 0.4. For instance, at $Ra_- = 10^6$ the air-wetted Nusselt number with $\gamma = 0.4$ is enhanced more than 60% in comparison with that with $\gamma \leqslant 0.3$. This interesting finding is further evidence reflecting the coupling between the convection heat transfer in the air and water layers within the annulus in the presence of the density inversion effect.

Experimental results

Representative interferograms obtained for the annulus partially filled with various volumetric fractions of water are shown in Fig. 9. A look at the interferograms for $\gamma = 0.5$ and $Ra_- = 19490$ clearly attests the numerical finding detected in Fig. 5 that the lowering of the air/water interface tends to further promote the density inversion effect as demonstrated by an evolution from a rather concentric fringe pattern at $d = -1.625$ to that featuring a downward hot plume activity at $d = 0.325$ in Fig. 9. It may also be inferred from such a sequence of changing fringe patterns that the flow in the water layer experiences a variation from a bicellular structure into the one dominated by a reversed buoyant recirculation as that predicted in Fig. 5.

In Fig. 10 the data for the measured local Nusselt number (the symbols) on the water-wetted portion of the inner cylinder are displayed to elucidate the influence of the air/water interface position at three different values of the density inversion parameter. For $\gamma = 0.2$, it is clear from the figure that the local heat transfer rate on the water-wetted surface decreases with the lowering of the interface; and a monotonic decrease from the bottom until the interface can be detected, signifying a clockwise convective flow. On the other end, at $\gamma = 0.7$ the variation trend of the local Nusselt number appears to be reversed, a further indication of the occurrence of the convective inversion phenomenon. Yet the data for $\gamma = 0.5$ exhibit somewhat of a transition between that for $\gamma = 0.2$ and 0.7. Furthermore, the sudden drop-off of the local Nusselt number shown in Fig. 10 for $\gamma = 0.7$ is attributed to the separation of the boundary layer below the interface. Above all, the measured heat transfer results displayed in Fig. 10 clearly demonstrate that the lowering of the air/water interface may induce significant heat transfer enhancement on the water-wetted inner cylinder in the presence of the density inversion phenomenon.

For comparison, also included in Fig. 10 are the corresponding numerical predictions (the lines) for the water-wetted Nusselt number on the inner cylinder. It appears that there exists a good agreement between the predicted and the experimental results for the local Nusselt number, lending further support to the numerical formulation adopted in the present study.

Finally, Fig. 11 conveys the relation between the measured data of the water-wetted average Nusselt number and the density inversion parameter at different values of d. The measured average heat transfer data clearly attest the existence of a minimum value at certain critical values of the density inversion parameter, depending on the value of d. The critical value of the inversion parameter yielding the minimum heat transfer rate appears to be about 0.45 and 0.4 for negative and positive values of d, respectively. Furthermore, it can be seen from the figure that changing the air/water interface position has a significant influence on the average water-wetted Nusselt number. In particular, the situation having the interface flush with the top of the inner cylinder, $d = 0.62$, always leads to the smallest average Nusselt number. This may be due to the fact that the heat transfer area for the water-wetted portion of the inner cylinder remains unchanged until interface lowering flush with the top of the inner cylinder and therefrom starts to decrease with further lowering of the interface. A further examination of Fig. 11 reveals that for $\gamma \geqslant 0.45$, namely under the dominance of the density inversion effect, the lowering of the interface below the top of the inner cylinder consistently yields an enhanced average water-wetted heat transfer rate.

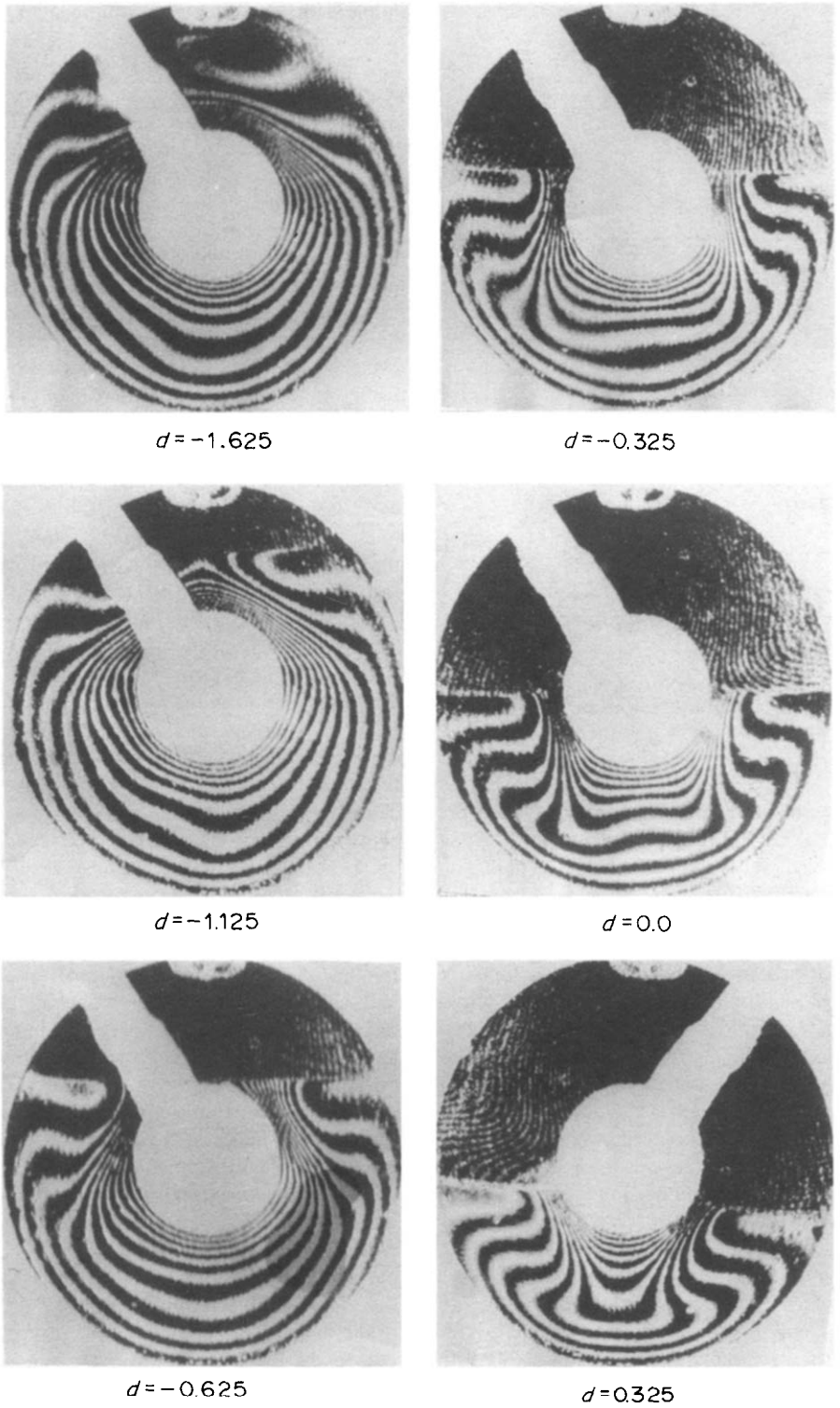

FIG. 9. Typical interferograms for an annulus filled with various volumetric fractions of water at $Ra_{-} = 19\,490$ and $\gamma = 0.5$.

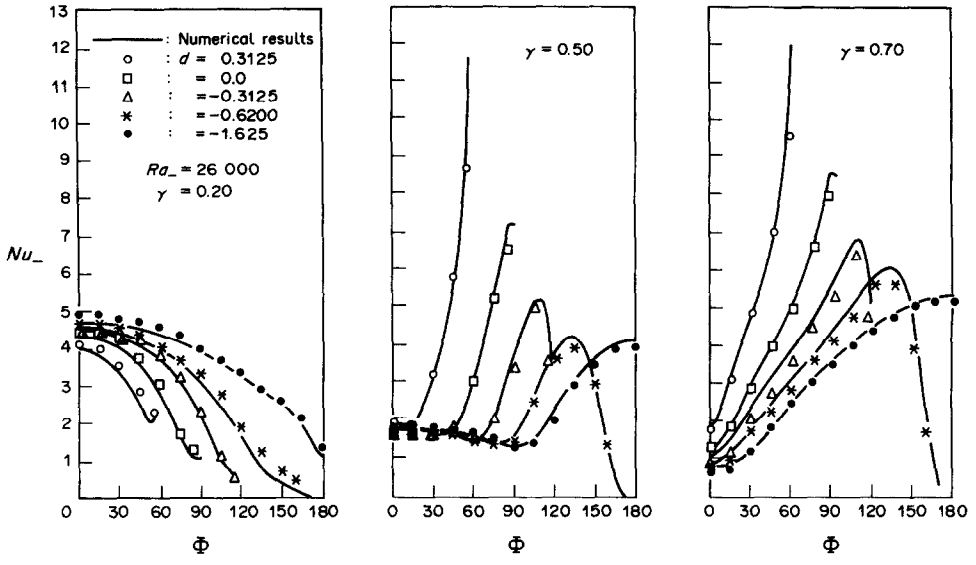

FIG. 10. Distribution of local Nusselt number on the water-wetted portion of the inner cylinder.

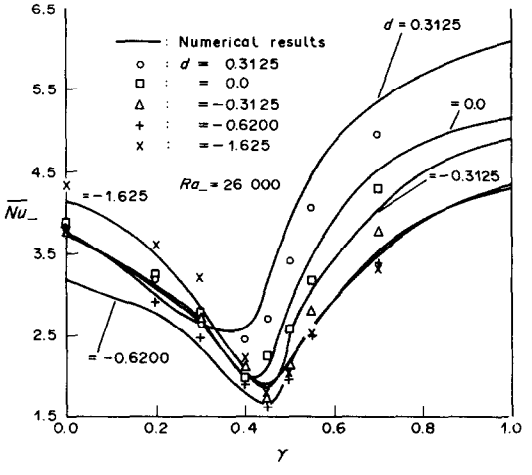

FIG. 11. Comparison of predicted results for the water-wetted average Nusselt number with the experimental data.

Also included in Fig. 11 are the numerical predictions for the corresponding experiments. Comparisons between the measured data and predicted results show a good agreement in the variation trends, but with a discernible quantitative discrepancy. The discrepancy may in part be due to the uncertainty in evaluation of the heat transfer area associated with the meniscus of the air/water interface in contact with the surface of the inner cylinder as well as the heat exchange of the test cell with the ambient environment.

CONCLUDING REMARKS

A combined numerical and experimental study of natural convection inside a horizontal concentric cylindrical annulus partially filled with cold water has been performed. Both the numerical and the experimental results obtained in the present study unveil an interesting coupling between the natural convection developed in the air layer and that in the water bulk in the presence of the density inversion phenomenon. The occurrence of the convective inversion phenomenon in the cold water region induces a step-function-like increase of heat transfer on the air-wetted portion of the inner cylinder. On the other hand, the intensified natural convection in the air layer with increasing Rayleigh number may further evoke the occurrence of the density inversion phenomenon in the water bulk. Furthermore, it is found that the lowering of the air/water interface has a somewhat similar effect to that of increasing Rayleigh number on the density inversion phenomenon in the cold water region of the annulus.

The predictions based on the mathematical formulation neglecting the surface tension effect are found to be in good agreement with the experimental data.

Acknowledgement—This research has been supported by the National Science Council of the Republic of China through Grant No. NSC79-0401-E006-04. Computer facilities were made available by the National Cheng Kung University Computing Centre.

REFERENCES

1. B. Gebhart, Boundary region transport in cold pure and saline water. In *Natural Convection: Fundamentals and Applications* (Edited by S. Kakac, W. Aung and R. Viskanta), pp. 987–1009. Hemisphere, Washington, DC (1985).
2. U. Projahn and H. Beer, Theoretical and experimental study of transient and steady-state natural convection heat transfer from a vertical flat plate partially immersed in water, *Int. J. Heat Mass Transfer* **28**, 1487–1498 (1985).
3. U. Projahn and H. Beer, Thermogravitational and thermocapillary convection heat transfer in concentric and

eccentric horizontal cylindrical annuli filled with two immiscible fluids, *Int. J. Heat Mass Transfer* **30,** 93–107 (1987).
4. C. J. Ho and Y. H. Lin, Thermal convection heat transfer of air/water layers enclosed in horizontal annuli with mixed boundary conditions, *Wärme- und Stoffübertr.* **24,** 211–224 (1989).
5. B. Gebhart and J. Mollendorf, A new density relation for pure and saline water, *Deep-Sea Res.* **24,** 831–848 (1974).
6. B. P. Leonard, A convectively stable third-order accurate finite-difference method for steady two-dimensional flow and heat transfer. In *Numerical Properties and Methodologies in Heat Transfer* (Edited by T. M. Shih), pp. 211–226. Hemisphere, Washington, DC (1983).
7. W. Aung and R. O'Regan, Precise measurement of heat transfer using holographic interferometry, *Rev. Scient. Instrum.* **42,** 1755–1758 (1971).
8. W. Hauf and U. Grigull, Optical methods in heat transfer. In *Advances in Heat Transfer* (Edited by J. P. Hartnett and T. F. Irvine), Vol. 6, pp. 133–366. Academic Press, New York (1970).
9. D. White, R. Viskanta and W. Leidenfrost, Heat transfer during the melting of ice around a horizontal isothermal cylinder, *Exp. Fluids* **4,** 171–190 (1986).
10. T. H. Kuehn and R. J. Goldstein, An experimental and theoretical study of natural convection in the annulus between horizontal concentric cylinders, *J. Fluid Mech.* **74,** 695–719 (1976).
11. C. J. Ho and Y. H. Lin, Natural convection heat transfer of cold water within an eccentric horizontal cylindrical annulus, *ASME J. Heat Transfer* **110,** 894–900 (1988).

CONVECTION NATURELLE DANS UN ESPACE ANNULAIRE HORIZONTAL PARTIELLEMENT REMPLI D'EAU FROIDE

Résumé—On rapporte une étude combinée numérique et expérimentale de la convection naturelle dans un espace horizontal entre deux cylindres concentriques, partiellement rempli d'eau froide avec inversion de densité. L'interférométrie holographique est employée pour connaître la distribution de température dans la couche d'eau et un système de visualisation à ombre est utilisé pour mesurer le coefficient local de transfert thermique sur le cylindre intérieur de l'espace annulaire. On a conduit aussi des simulations numériques pour la convection laminaire, naturelle, permanente, des couches air/eau dans l'espace annulaire. Les résultats numériques et expérimentaux révèlent un couplage intéressant entre la convection naturelle de la couche d'air et celle de l'eau froide en présence de l'effet de l'inversion de densité. Les prédictions sont en bon accord avec les données expérimentales.

NATÜRLICHE KONVEKTION IN EINEM WAAGERECHTEN, TEILWEISE MIT KALTEM WASSER GEFÜLLTEN RINGRAUM

Zusammenfassung—Es wird eine kombinierte numerische und experimentelle Untersuchung vergestellt, in der die natürliche Konvektion innerhalb eines teilweise mit kaltem Wasser gefüllten, konzentrischen, horizontalen, zylindrischen Ringraums behandelt wird. Dabei wird die Dichteinversion berücksichtigt. Zur Darstellung der Temperaturverteilung in der Wasserschicht wird die holographische Interferometrie eingesetzt, zur Ermittlung der örtlichen Wärmeübergangskoeffizienten an der wasserbenetzten inneren Wand des Ringraums ein Laser-Schatten-Verfahren. Die stationäre, laminare, natürliche Konvektion in den Luft/Wasserschichten im Ringraum wird zusätzlich numerisch untersucht. Sowohl die numerischen als auch die experimentellen Ergebnisse der vorliegenden Untersuchung zeigen eine interessante Koppelung zwischen der natürlichen Konvektion in der Luftschicht und derjenigen im kalten Wasser, wenn die Dichteinversion auftritt. Die Ergebnisse von Berechnung und Experiment stimmen gut überein.

ЕСТЕСТВЕННАЯ КОНВЕКЦИЯ В ГОРИЗОНТАЛЬНОМ КОЛЬЦЕВОМ КАНАЛЕ, ЧАСТИЧНО ЗАПОЛНЕННОМ ХОЛОДНОЙ ВОДОЙ

Аннотация—Численно и экспериментально исследуется естественная конвекция в горизонтальном кольцевом канале, частично заполненном холодной водой, в температурном диапазоне, включающем температуру инверсии плотности. Для получения распределения температур в слое воды используется голографическая интерферометрия, а для измерения локального коэффициента теплопереноса на омываемом водой внутреннем цилиндре кольцевого канала применяется лазерная теневая система. Проводится численное моделирование стационарной ламинарной конвекции в слоях воздуха и воды, заполняющих кольцевой канал. Как численные, так и экспериментальные данные, полученные при исследовании, раскрывают интересную взаимосвязь между естественной конвекцией в слое воздуха и в объеме холодной воды при наличии эффекта инверсии плотности. Результаты расчетов хорошо согласуются с экспериментальными данными.